ACS APPLIED MATERIALS & INTERFACES

Research Article

www.acsami.org

# Film Confinement Induced "Jump-Percolation" Wetting Transition in Amphiphilic Block Copolymer Films

Namrata Salunke,[†] Asritha Nallapaneni,[†] Guangcui Yuan,[†,‡] Christopher M. Stafford,[‡] Hui Niu,[§] Matthew D. Shawkey,[∥] R. A. Weiss,*[,†] and Alamgir Karim*[,†,⊥]

[†]Department of Polymer Engineering, The University of Akron, 250 South Forge Street, Akron, Ohio 44325-0301, United States
[‡]National Institute of Standards and Technology, Gaithersburg, Maryland 20899, United States

Supporting Information

**ABSTRACT:** We report a first-order like sharp surface wettability transition with varying film thickness dependent morphology in cast films of an amphiphilic triblock copolymer. Films composed of poly(2-(*N*-ethylperfluorooctanesulfonamido) ethyl methyl acrylate), poly(FOSM), and poly(*N*,*N*′-dimethyl acrylamide), poly(DMA), with thickness ($h$) in the transition-range, $200 < h < 300$ nm, exhibited an abrupt hydrophobic to hydrophilic dynamic water contact angle transition. After an induction time, $t_i \approx 40$ to 180 s, water contact angle varied as $\theta_c \approx 116°$ to 40° with an ultrafast contact angle decay time constant, $\frac{d\theta_c}{dt} \approx -18°/s$. This behavior is a result of competing heterogeneous and antagonistic effects of bumpy poly(DMA) wetting domains against a nonwetting planar poly(FOSM) background, with a "jump percolation" wetting transition when the poly(DMA) domain density reaches unity. Outside of this film thickness range, relatively shallow decreasing water contact angle gradients were observed with a monotonically increasing poly(DMA) domain area coverage with increasing film thickness in the overall range of 40 nm (hydrophobic, $\theta_c \approx 118°$) $< h <$ 500 nm (hydrophilic, $\theta_c \approx 8°$). The optical diffuse reflectance properties of these rough surfaces exhibit an onset of diffuse reflectance maxima correlated to the transition morphology film thickness.

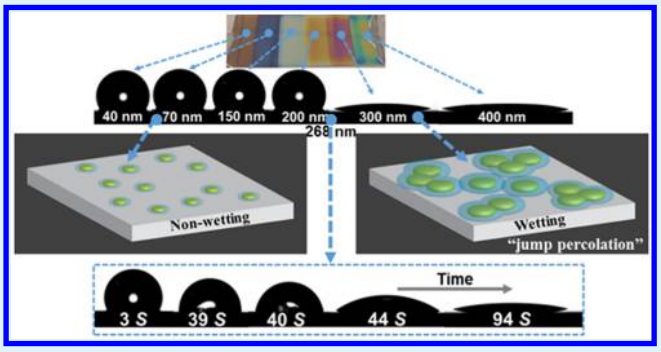


**KEYWORDS:** *confinement effects, hydrophobicity, hydrophilicity, jump percolation*

## 1. INTRODUCTION

Controlling surface wettability has been the subject of extensive study due to the need for developing materials and coatings with properties such as, self-cleaning surfaces with enhanced hydrophobic,[1] hydrophilic, or oleophobic[2] characteristics. Small changes in the synergy of surface chemistry and morphology can lead to dramatic changes in surface wettability, enabling the creation of surface wettability gradients, in some cases ranging from superhydrophobic to superhydrophilic.[3] Approaches to manipulate surface chemistry include self-assembled monolayer (SAM) deposition,[4,5] plasma treatment,[6] utilization of photosensitive materials,[7] direct current corona discharge,[8] and chemical treatments.[9−11] Alternate techniques rely on regulating the surface morphology by roughening,[12] nanopatterning,[13] and multilength-scale patterning.[14] Techniques that combine multiple approaches have also been developed.[12] In this paper we use an amphiphilic block copolymer (BCP) to achieve a controlled surface wettability gradient.

BCPs offer attractive properties due to their ability to self-assemble[15] into various nanodomain morphologies such as cylinders, lamellae, spheres, and gyroids.[16] In this regard, block copolymers are known to form ordered structures as well as micelles when cast from selective solvents for a constituent block. Several efforts have been made to control this self-assembly,[17] specifically the formation of micelles for drug delivery applications,[18] novel optical properties,[19] or to obtain functionalized surfaces.[20]

This paper reports the surface wettability of thin hydrogel films obtained from self-assembled amphiphilic block copolymers. Such surfaces with varying surface wettabilities are ideal for studies on cell growth[21] and platelet and protein adsorption.[22] These surfaces are also attractive for understanding the fundamentals of droplet motion which has been studied experimentally[23,24] and by simulation[25,26] for microfluidic applications.[27] Amphiphilic copolymers are also being used to obtain surfaces with switchable wettabilities triggered by external stimuli such as variation of pH or exposure to water.[28−30] A physical network, FDF triblock copolymer hydrogel[31] was used in the present study, where F and D denote poly(2-(*N*- ethylperfluorooctanesulfonamido-sulfonamido) ethyl methyl acrylate) or poly(FOSM), and poly(*N*,*N*′-dimethyl acrylamide) or poly(DMA), respectively, Figure 1.

Received: May 22, 2017
Accepted: September 19, 2017
Published: September 19, 2017




DOI: 10.1021/acsami.7b07245
ACS Appl. Mater. Interfaces 2017, 9, 35349−35359

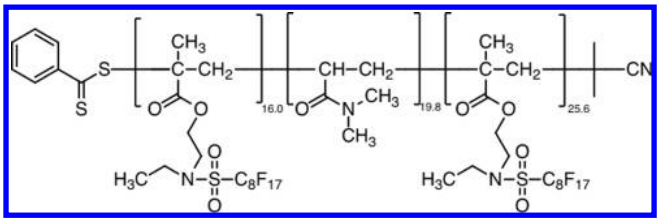

**Figure 1.** Chemical structure of FDF. The end-groups are remnants of the reversible addition−fragmentation chain-transfer (RAFT) agent used.

The FDF block copolymer is amphiphilic, since poly(FOSM) is hydrophobic and poly(DMA) is hydrophilic. When a physical network of such copolymers comes in contact with water, the hydrophobes can rearrange by aggregating to form nanoscale clusters[32,33] that act as dynamic multijunction cross-links while the hydrophilic phase absorbs water and swells to form a hydrogel. Niu et al.[31] reported the synthesis and characterization of the structure and bulk properties of the FDF hydrogels, but the thin film characteristics of the materials have not been investigated.

In this paper, we explore the effect of film thickness on microstructure, morphology, surface chemistry, and surface wetting properties of FDF block copolymer thin films. Amphiphilic BCP films were prepared by a one-step solvent casting process, and the bulk microstructure along with the phase-separated surface morphology form by molecular self-assembly, all during the film casting and drying process. We show that a dynamic surface wettability transition, marked by a rapid substantial change in the measured water contact angle, $\theta_c$, occurs over a range of film thickness from 200 to 300 nm. For thinner and thicker films, the BCP surfaces are hydrophobic or hydrophilic respectively, and $\theta_c$ changes only slightly with increasing film thickness. Aside from the novel wettability properties, the scale of domain phase separation on the film surface also affected the diffuse reflectance properties of the films.

## 2. RESULTS AND DISCUSSION

**2.1. Initial Quasi-static Contact Angle Regime.** Figure 2 shows the measured water contact angle at short times after placement of water drops ($t_{measure} \approx 240$ s, $t_{measure}$ being the time at which measurement was recorded after the water drop was first placed on the substrate) on FDF flow-coated thin films with varying multistep film thickness, $h \approx 40$ to 400 nm on a single silica substrate. All the experiments described in this paper were performed on as-cast dry FDF films. The different colors seen in the film shown in Figure 2 are from variation in thickness observed due to interference of visible light. The films were hydrophobic ($\theta_c > 90°$) for film thickness, $h \leq 200$ nm, but when $h > 300$ nm, the water contact angle decreased dramatically to $\theta_c \leq 10°$, which indicates that the surface became hydrophilic. This variation in surface wettability is attributed to the confinement induced self-assembly property of poly(DMA) domains at the BCP film surface as discussed in more detail in the paper. All contact angles have an error of ±2° (confidence interval ≥95%), while the film thickness error is ±5 nm for $h < 300$ nm and ±10 nm for $h > 300$ nm (confidence intervals ≥95%)

**2.2. Dynamic Contact Angle Regime.** The temporal behavior of the water contact angle, $\theta_c(t)$ on the dry FDF surfaces varied with film thickness, as shown in Figure 3(i) for the full range of film thickness with $75 \leq h \leq 543$ nm. Figure 3(i-a) is a magnified image showing a contact angle snapshot for $t \leq 45$ s. The observed trend indicated that overall, the water droplet wetting behavior changed from hydrophobic to hydrophilic with increasing thickness following a finite induction time ($t_i$) that denotes the knee-point for the contact angle to drop in time. The films were divided into three regimes depending on their wetting dynamics, as illustrated in Figure 3(ii)—hydrophobic to hydrophilic contact angle transition time ($\tau$) relating to contact angle decay, as well as rate of contact angle drop ($\frac{d\theta_c}{dt}$) were used to classify the different regimes. The data for contact angles at specific times, $\theta_c(t)$, during the transition from hydrophobic to hydrophilic behavior of the surface for the different film thicknesses shown in Figure 3(i) contact angle variation with time were fit to an exponential decay, eq 1:

$$\frac{\theta_c(t)}{\theta_{co}} = e^{-t/\tau} \tag{1}$$

The transition time for the contact angle decay, $\tau$, defined as the time when $\theta_c(t)/\theta_{co} = e^{-1} = 0.368$, where $\theta_{co}$ is the water contact angle at the beginning of the transition.

*2.2.1. Hydrophobic Regime.* Films with $h \leq 200$ nm showed hydrophobic behavior with a gradual drop in contact angle, $\frac{d\theta_c}{dt} \approx -0.04°/s$, over the 240 s duration of the experiment, Figure 3(i). The decrease of contact angle is due to evaporation of water from the droplet and therefore is an apparent receding contact angle, which is typically less than the static contact angle, so that the film behaves like a "regular" polymer film surface. A more detailed explanation is provided later. Over the time period of the droplet drying process, these films did not show any wettability transition.

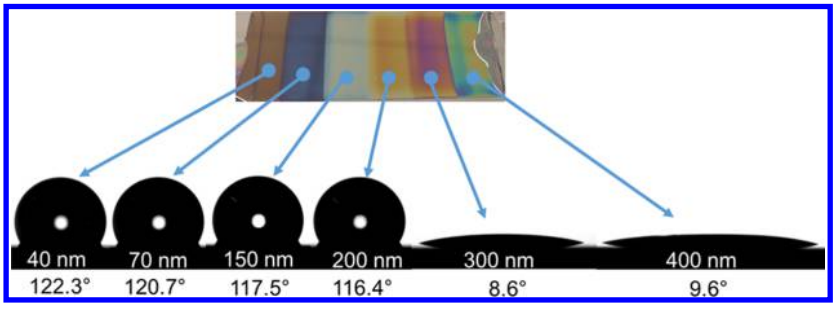


**Figure 2.** FDF films of various thickness (in white font) with snapshots of equilibrium water drop at $t_{measure} \approx 240$ s, and contact angle given by the numbers written under corresponding images. The film surface dimensions of each thickness step is 2.5 × 1 cm$^2$.


DOI: 10.1021/acsami.7b07245
ACS Appl. Mater. Interfaces 2017, 9, 35349−35359

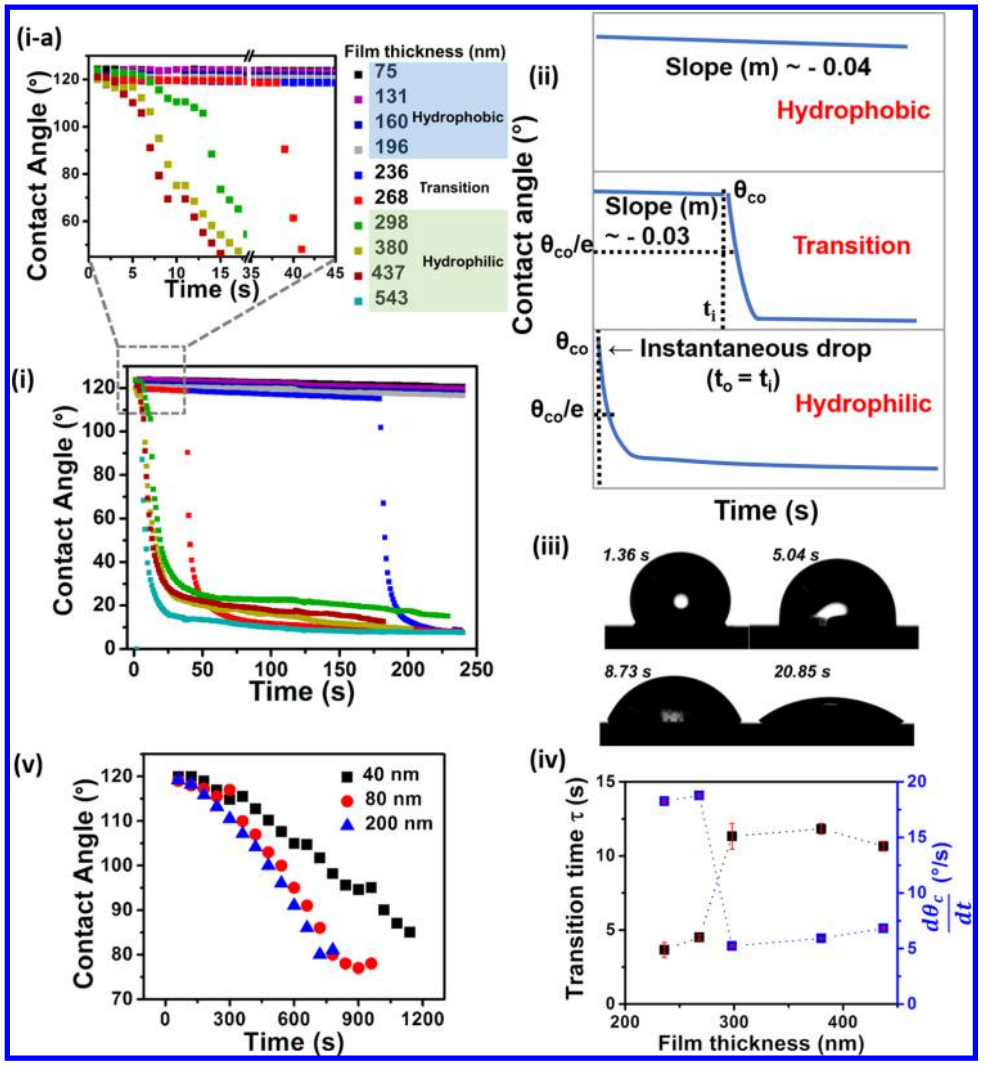


**Figure 3.** Clockwise: (i) Water contact angle dynamics for different film thickness; (i-a) is the zoom-in of (i) showing contact angle dynamics for $t \leq$ 45 s. The time and thickness dependent properties were classified as three different regimes of wetting behavior, hydrophobic, transition, and hydrophilic. Schematic (ii) shows details of the classification. (iii) Snapshots of water contact angle as a function of time on a 400 nm film; (iv) transition time, $\tau$ (black) and rate of transition contact angle drop, $\frac{d\theta_c}{dt}$ (blue) as a function of film thickness (error bars represent standard error); and (v) contact angle at long times for hydrophobic films, apparent recede observed due to evaporation of water.

*2.2.2. Transition Regime.* This regime included films with approximately $236 \leq h < 300$ nm. In this case, a first-order like sharp drop in contact angle was observed following an induction time ranging from $t_i$ = 40 to 180 s. In general, during the induction period, the slope of the hydrophobic region ($t \leq t_i$) was $\frac{d\theta_c}{dt} \approx -0.03°/s$ for all films, which again was due to water evaporation and related to a measure of receding contact angle.

*2.2.3. Hydrophilic Regime.* For even thicker films with $h \geq$ 298 nm, the initial $\theta_{co} \approx 118°$, indicative of a hydrophobic surface. However, the surface rapidly became hydrophilic, $\theta_c <$ 30°, within 12 s of addition of the water drop to the film surface corresponding to a contact angle change rate of $\approx -5°/s$, much faster than the drop evaporation rate in the hydrophobic regime. Thus, it must correspond to some surface dynamics, either in drop spreading or film topography rearrangement. Following this hydrophobic to hydrophilic transition of the film surface, the hydrophilic nature of the surface (i.e., decreasing $\theta_c$) continued to increase, but at a much slower rate to $\theta_c \approx 10°$ over a period of 50 to 200 s. This corresponds to a contact angle rate change of approximately $-0.05°/s$, consistent with a drop evaporation rate in this latter phase of contact angle evolution.

Photos of the time evolution of the water droplet shape on a 400 nm thick film are shown in Figure 3(iii). The hydrophobic to hydrophilic transition was observed almost immediately after the droplet was placed on the FDF film surface. The transition times were calculated using contact angle ($\theta_{co}$) at $t_o$ which is the initial point of the rapid decrease of the contact angle. The induction time for the hydrophobic to hydrophilic transition decreased with increasing film thickness. The dependence of drop rate time exponent $\tau$ on the thickness of the FDF films that showed a hydrophobic to hydrophilic transition is shown in Figure 3(iv). We observe an increase in $\tau$ from $h \approx 268$ to $h \approx 298$ nm, above which it appeared to be thickness independent. The rate of the contact angle drop during the hydrophobic to hydrophilic transition, ($\frac{d\theta_c}{dt}$), also showed two distinct regimes, Figure 3(iv). Films in the transition regime showed a high rate of contact angle decrease, $\frac{d\theta_c}{dt} \approx -18°/s$,


DOI: 10.1021/acsami.7b07245
ACS Appl. Mater. Interfaces 2017, 9, 35349−35359

while films in hydrophilic regime showed lower values, $\frac{d\theta_c}{dt} \approx -5°/s$.

**2.3. Final Quasi-static Contact Angle Regime.** The films in the hydrophobic regime did not undergo a hydrophobic to hydrophilic transition. The apparent second-order like transition shown in Figure 3(v) is actually an artifact due to evaporation of the water from the droplet, and the consequential decrease in the droplet size which makes it appear that the film became hydrophilic at long times. This phenomenon was also reported by Bexon et al.[34] and Bourges-Monnier et al.,[35] who explained that during evaporation the contact radius remains constant due to molecular pinning, and the associated reduction in drop height produces the apparent reduction in contact angle. The same phenomenon explains the results in Figure 3(v), and the absence of any change in the wetting behavior was confirmed by adding a fresh water droplet to the FDF film after 600 s (when contact angle measurement of the original droplet appeared to indicate that the film had become hydrophilic, see Figure 3(v)). The fresh drop exhibited the same contact angle of ∼119° as did the original drop when first added to the 70 nm film.

It is tempting to attribute the $h$-dependence of $\tau$ to the relaxation behavior of the film. One hypothesis is that the fluorinated nanodomains rearrange due to the presence of the water droplet, which allows more of the hydrophilic poly(DMA) phase to be exposed at the film−water interface. The hydrophilic poly(DMA) favors spreading of water on the film surface, which lowers $\theta_c$. A few studies have observed such a dynamic water contact angle on a copolymer film, and have attributed this to structural rearrangement at the surface.[36−40] Three studies in particular (Lee et al.,[36] Crowe-Willoughby et al.,[37] and Vaidya et al.[38]) observed a temporal hydrophobic−hydrophilic surface wettability transition. Lee et al.[36] reported time-dependent contact angle behavior for alternating multilayer films of poly(ethylene glycol)-functionalized poly(vinyl alcohol) and poly(acrylic acid) prepared by layer-by-layer assembly. In their case, an initial water contact angle of 117° dropped to 50° in 600 s, which appeared to include the induction and transition times, that are considered separate in the present study. The films used in ref 36 were also much thicker, > 1.5 $\mu$m, than the films considered in this paper. The high initial water contact angle was explained as a consequence of hydrophobic acetate groups present in the partially hydrolyzed PVA that were expected to be trapped at the film surface. Vaidya et al.[38] studied films of polyurethane which were modified to include segments of perfluoropolyether (PFPE), polydimethylsiloxane (PDMS) and polyethylene glycol (PEG). They observed a hydrophobic−hydrophilic water contact angle transition in a duration of ∼20 min. They attributed this behavior to the hydrophobic PFPE groups phase separating to the surface while dragging the hydrophilic PEG segments along with them, thus allowing the latter to form a subsurface layer. In the presence of water, the subsurface layer rearranges at the film−water interface making the surface hydrophilic. Theato et al.[41] used near edge X-ray absorption fine structure (NEXAFS) to track surface reorganization in an amphiphilic diblock copolymer film comprising poly(styrene)−block−poly(4-(2-(2-(2-acetoxy)ethoxy)ethoxy)styrene) in the presence of water. No contact angles were reported, but they observed that the surface layer exhibited an exchange between the hydrophobic and hydrophilic groups when exposed to water. The present FDF study shares some apparent similarity to the system of Vaidya et al.,[38] since the BCP domains containing the hydrophilic poly(DMA) chains form a subsurface layer due to its higher surface energy while the lower surface energy hydrophobic poly(FOSM) domains reside at the air surface under ambient conditions. Presumably, reorganization of poly(DMA) to the film surface takes place in the presence of water.

Haraguchi et al.,[42−44] showed a dynamic water contact angle transition in nanocomposite hydrogels consisting of poly(*N*-isopropylacrylamide) with varying amounts of clay. The nanocomposite hydrogels showed contact angles ranging from hydrophobicity (due to the presence of *N*-isopropyl groups) to hydrophilicity depending on the network density. At intermediate clay concentrations, they observed an abrupt water contact angle transition occurring several minutes after the water drop is placed on the sample surface. This was attributed to absorption of water by the gel. Although the current FDF system shows a similar dynamic water contact angle transition, the relatively faster transition is likely occurring due to chain rearrangement at the surface.

Several other studies observe a dynamic water contact angle as a consequence of surface restructuring, but the film thickness dependent hydrophobic−hydrophilic transition is absent.[39,40] Wang et al.[40] studied the surface properties of poly(2-(*N*,*N*-dimethylamino)ethyl methacrylate) and poly(1-(1H,1H,2H,2H-perfluorodecyloxy)-3-(3,6,9-trioxadecyloxy)-propan-2-yl acrylate) block copolymers, a fluorinated BCP similar to the present study, with varying molecular weights. They observed dynamic water contact angle measured over 30 s, but in their case, the hydrophobic systems remained hydrophobic, and the hydrophilic systems remained hydrophilic at the end of the experiment. However, a shallow drop in water contact angle was observed in all cases, attributed to surface rearrangement. Thus, it appears there is a fundamental difference between our systems and such surface rearranging systems. In our case, the presence of macroscopic wetting domains in a background of nonwetting matrix can exhibit large dynamic contact angle change as shown later in the paper.

For FDF films in the transition regime, the extent of the hydrophobic to hydrophilic transition was ≈3.5 s and $\frac{d\theta_c}{dt} \approx -18°/s$. This rate of contact angle decrease was ultrafast compared to the other reports of contact angle dynamics, where the transition time varied from 10 s to several minutes,[36−38] and the fastest contact change was $\frac{d\theta_c}{dt} = -2°/s$.[37] These results indicate that whatever similarity there may be in the structural reorganization of the various studies showing a dynamic hydrophobic to hydrophilic transition, the structural changes in the FDF film are either faster or invoke alternate mechanisms than in the other films. These may be a consequence of the dual combination of a larger difference in the polarity between the phases in the FDF films, as well as the large dimensions of individual poly(DMA) phases.

When a BCP is solution-cast upon a surface, depending on the substrate surface energy, one block preferentially wets the substrate allowing the second block to form a layer on top of it during the solvent drying process.[45] Surface energies of the individual components of the FDF BCP were estimated to be $\gamma_{poly(FOSM)} = 22$ mJ/m$^2$ and $\gamma_{poly(DMA)} = 73$ mJ/m$^2$ using Fowkes Theory[46] which relies on dispersive and polar components of the homopolymers for estimation of surface energy. As the films were cast onto UVO treated silicon wafers of $\gamma = 76$ mJ/m$^2$, the higher surface energy poly(DMA) phase was expected


DOI: 10.1021/acsami.7b07245
ACS Appl. Mater. Interfaces 2017, 9, 35349−35359

to wet the silica substrate, and the low surface energy, hydrophobic poly(FOSM) blocks should segregate to the film-air interface. This asymmetric substrate and air surface wetting effect should facilitate orientation of the microphases parallel to the substrate and allow the low surface energy fluorinated nanodomains to assemble on the surface of very thin films. In reality, however, as the film thickness increases, the correlation between parallel domains (out-of-plane z-phase separation) may be lost due to an increasing tendency for in-plane (x-y) phase separation as the film thickness approaches a more bulk like structure where surface effects are diminished.

The surface and film interior nano and mesoscale structure was confirmed by a combination of X-ray reflectivity (XRR), grazing incidence small-angle X-ray scattering (GISAXS), and correlating these to the real-space atomic force microscopy (AFM) images of the film surface. GISAXS is an X-ray scattering technique used to determine the BCP domain spacing and orientation morphology simultaneously in both out-of-plane and in-plane. In this technique, X-rays are incident at very low angles just grazing the film surface and scattering data are collected using a 2D detector at a specular angle. The grazing angle is varied typically so that only the top film surface is probed below a critical angle, as well as the film interior at higher grazing angles. A GISAXS image for a 70 nm FDF film is shown in Figure 4(i) where $\alpha = 0.18°$ (the critical angle in air,

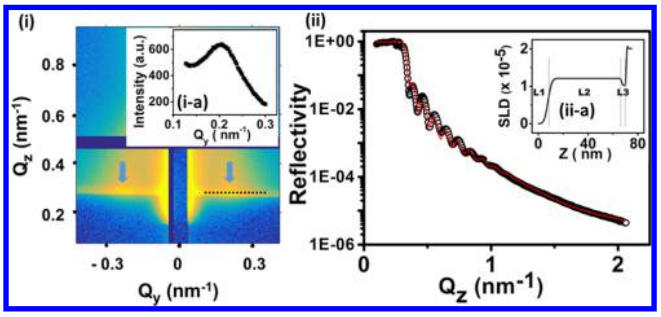


**Figure 4.** (i) GISAXS at critical angle and inset (i-a), the corresponding in-plane line cut (dashed line) (ii) X-ray reflectivity data (symbols), fit (solid line) and inset (ii-a), the corresponding model depicted by scattering length density (SLD) as a function of film depth for a 70 nm film. Z = 0 nm denotes the film−air interface.

$\alpha_c = 0.15°$ for FDF) At this angle, the entire film "interior", i.e., beyond the top 10 nm of film surface is being probed. The broad in-plane ($Q_y$−direction) Bragg peak (line-cut shown in the inset, Figure 4(i-a)), corresponds to the BCP domain size ($L_o \approx 31$ nm). The Bragg peak values agree well with the domain size of the lamellae for this BCP as previously measured by small-angle X-ray scattering (SAXS) by Niu et al. in Weiss group.[31] However, the broad low-intensity peaks in GISAXS shown by blue vertical arrows indicates some component of weakly ordered vertical domain orientation in the film interior. The low-intensity and lack of peak sharpness imply lack of domain correlation and short persistence lengths respectively, which is expected in a quenched partially ordered system. Similar results were observed for films with different thicknesses (the GISAXS images are provided in the Supporting Information, SI, Figure S1) where broad, low-intensity vertical peaks are observed. Scherrer analysis[47] (eqs 2 and 3) was performed to estimate a domain correlation length (block copolymer grain size with a given orientation) $\zeta$, which is defined more broadly as the length scale over which the position and orientation of a self-assembled morphology is preserved.

$$\zeta = \frac{2\pi K}{\Delta q} \tag{2}$$

$$\Delta q = \frac{4\pi}{\lambda}\cos(\theta)\frac{B}{2} \tag{3}$$

Here, $K$ is the Scherrer constant (defined as ~0.94),[47] $\lambda$ is the X-ray wavelength (1.6868 Å), $2\theta$ is the scattering angle and $B$ is the width of the Bragg peak, defined as the full width at half-maximum (fwhm). The Scherrer analysis, which is usually used for crystalline systems with sharp grain boundaries, was used here to estimate the domain correlation length, $\zeta$. For the 70 nm FDF film, $\zeta$ = 23.37 nm and the scaled correlation length ($\zeta/L_o$) as a measure of short or long-range order was calculated as 0.79 ± 0.04, which indicate small grain sizes or short-range order. Similarly, for 200 and 300 nm thick FDF films, $\zeta/L_o$ = 1.08 ± 0.06 and 1.06 ± 0.02, respectively, which indicates that for each film the grain size was approximately equal to the domain size. Confidence intervals are ≥95% in all cases.

X-ray reflectivity (XRR) was used to supplement the information at high $Q$ and to probe any out-of-plane ($Q_z$) structure at specular conditions ($Q_y$ = 0) which is difficult to resolve by GISAXS due to the presence of a beamstop. The XRR data and the corresponding model for a 70 nm film, shown in Figure 4(ii), indicate that no $z$ (out of plane)-ordering of substrate parallel multilayering of repeating domains, such as lamellae within the BCP nanostructure, occurred, as evident by the absence of Bragg peaks. The thin 70 nm sample showed only Kiessig film thickness oscillations, which is caused by interference from the film thickness at film−substrate and the film−air interfaces. Nevertheless, the $z$-film composition is nonhomogeneous for all film thicknesses, but one must keep in mind that XRR will average over any in-plane inhomogeneity, such as surface or internal in-plane domains inferred by GISAXS or AFM. The model (SLD profile) for this film, Figure 4(ii-a), shows three distinct layers: (1) a 7.8 nm thick poly(DMA) rich FDF layer (L1) at the film−air interface; (2) a 3 nm thick poly(DMA) wetting layer at the silica substrate (L3); and (3) the bulk of the film, ~59 nm (L2), that appears to be the BCP with no z (out-of-plane) ordering. SLD values of poly(DMA) and poly(FOSM) are determined to be $0.89 \times 10^{-5}$ Å$^{-2}$ and $1.27 \times 10^{-5}$ Å$^{-2}$, respectively. However, the SLD of poly(DMA) is higher as its hygroscopic nature allows it to take up water vapor from air and swells the film at ambient relative humidity (details presented in SI). The SLD of water is $0.9 \times 10^{-5}$ Å$^{-2}$, so the swollen film, specifically poly(DMA) will show an increased SLD. As the GISAXS results indicate that the bulk of the sample consists of weakly vertically oriented domains, we can conclude that L2 consists of these vertical domains with low grain size. XRR does not indicate which chemistry is present at the surface. The film surface L1 would be consistent with a mixed state of poly(DMA) rich domains and a notable fraction of poly(FOSM) chains driven to the film surface. This is essentially due to the presence of poly(DMA) domains at the film surface in a majority poly(FOSM) background as shown by AFM later.

One might reasonably expect that the fluorinated poly(FOSM) phase of the BCP is responsible for the surface hydrophobicity. Thus, the chemistry of the surface was probed by X-ray photoelectron spectroscopy (XPS) to evaluate


DOI: 10.1021/acsami.7b07245
ACS Appl. Mater. Interfaces 2017, 9, 35349−35359

whether changes in the fluorine content of the surface can explain the transition in the wetting behavior from hydrophobic to hydrophilic. In XPS, the X-rays penetrate only the top 7 to 10 nm of the film,[48] which provides a measure of the surface as opposed to the bulk composition. The XPS results are provided in Table 1. Although there is an overall decreasing trend in the

**Table 1. Elemental Composition of the Surface of FDF Films with Varying Film Thickness**

| | film thickness | | | | |
|---|---|---|---|---|---|
| atomic % | 40 nm | 70 nm | 200 nm | 300 nm | 400 nm |
| F 1s | 46.7 | 46.0 | 45.3 | 42.3 | 43.5 |
| C 1s | 39.9 | 40.2 | 40.3 | 44.0 | 42.6 |
| O 1s | 9.5 | 9.6 | 9.6 | 9.5 | 9.2 |
| N 1s | 2.5 | 2.3 | 2.5 | 2.7 | 3.1 |
| S 2p | 2.0 | 1.0 | 2.3 | 1.6 | 1.7 |

concentration of fluorine (F 1s), which is consistent with the increasing hydrophilicity observed for increasing film thickness, no abrupt change in the fluorine concentration was observed coincident with the hydrophobic to hydrophilic transition.

The possibility that changes in the surface morphology produced the wetting transition was assessed by imaging the surface morphology with AFM and determining how it varied with increasing film thickness. The AFM data in Figure 5 show circular domains at the surface of the films, whose size and density increased with increasing film thickness. These hemispherical surface domains are determined to be hydrophilic (polyDMA) micelles dispersed in a hydrophobic (polyFOSM) continuous phase, as determined from AFM-friction experiments discussed later in this paper. (We note that these structures on the film surface are not typical block copolymer lamellar islands as they do not have a rectangular topography consistent with domain height $L_o$).[49]

The reason for the effect of film thickness variation on the size of the poly(DMA) domains ("finite-size" effect) may be related to the phenomenon reported by Walheim et al.,[50] who observed that in the case of poly(styrene)/poly(methyl methacrylate) blends the lateral dimension of the PMMA domains at the film surface increased with increasing film thickness. They also determined that this variation in the lateral dimension of domains is a consequence of rate of solvent evaporation. Since thicker films took longer to dry, longer polymer diffusion times were available, which allow for a higher degree of phase separation following the film casting process.

The structure that emerges from the XRR, GISAXS, and AFM data is shown schematically in Figure 5(G), wherein there is a wetted poly(DMA) layer at the film−substrate interface (L3), weakly oriented perpendicular BCP microstructure in the bulk (L2), transitioning to a poly(DMA) micellar domains in a poly(FOSM) matrix at the surface (L1). The BCP domains size, $L_o$ is far smaller than the poly(DMA) micelle dimension which are 1 order of magnitude larger, so we believe the observed film topography is block copolymer surface micelles with the poly(DMA) micellar phase at the top surface as determined by AFM in contact mode, Figure 5 D, D1, and D2. (See Supporting Information for frictional AFM experimental details at varying relative humidity and surface modulus measurements, Figure S4. However, no significant variation in surface modulus with film thickness was observed.) We now try to understand why these surface structures result in the abrupt contact angle transition with increase of film thickness.

To this end, we perform a detailed analysis of the film surface structure in terms of surface roughness, micelle aspect ratio, and micelle area coverage on film surface with increasing film thickness. Figure 6 shows the effect of film thickness on the average height ($H_{micelles}$), the lateral dimension ($L_{micelles}$) of the poly(DMA) micelles, domain aspect ratio ($\beta$), and the area fraction ($A_{micelles}$) of the film surface covered by the hydrophilic micelles. The micelle height increased with film thickness, Figure 6(i). The maximum and minimum micelle heights ($H_{max}$ and $H_{min}$) are also plotted to observe the variation in micelle height, specifically at greater film thickness. A similar trend was

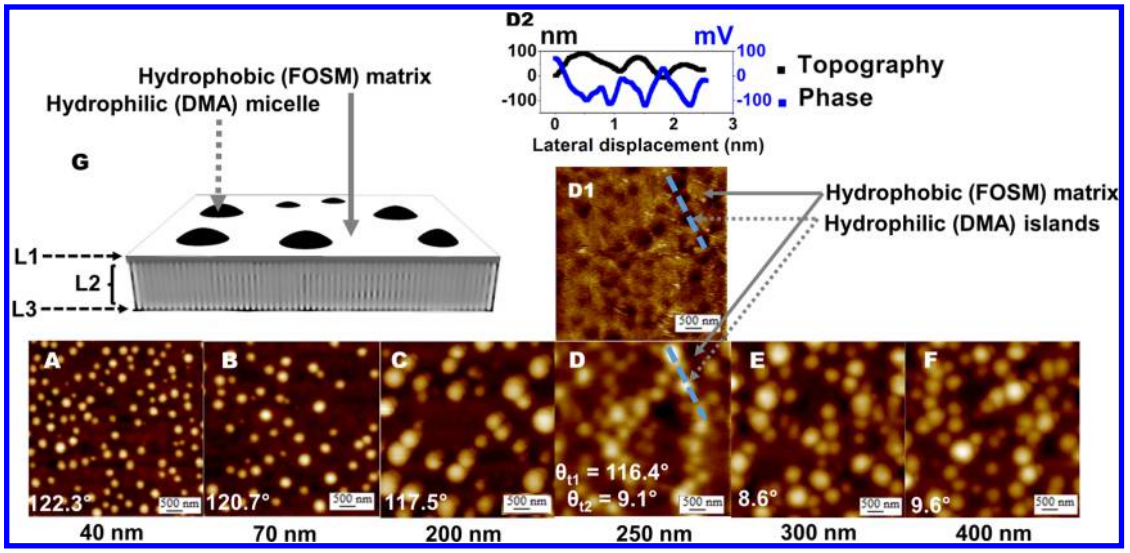


**Figure 5.** AFM images showing surface morphology i.e., topography images of as cast FDF films with increasing thickness. Film thickness and equilibrium contact angle are indicated for each image. For (D) 250 nm film, $\theta_{t1}$ and $\theta_{t2}$ represent equilibrium contact angles before and after transition. (D1) is the friction image corresponding to (D); (D2) shows line cut (dashed lines) profiles from the friction (D1) and topography images (D) for the 250 nm film. (G) Schematic of morphology predicted from AFM, XRR and GISAXS, black and white represent poly(DMA) and poly(FOSM) respectively, and the gray regions represent mixture of the two components. All contact angles have an error of ±2° (confidence interval ≥95%).


DOI: 10.1021/acsami.7b07245
ACS Appl. Mater. Interfaces 2017, 9, 35349−35359

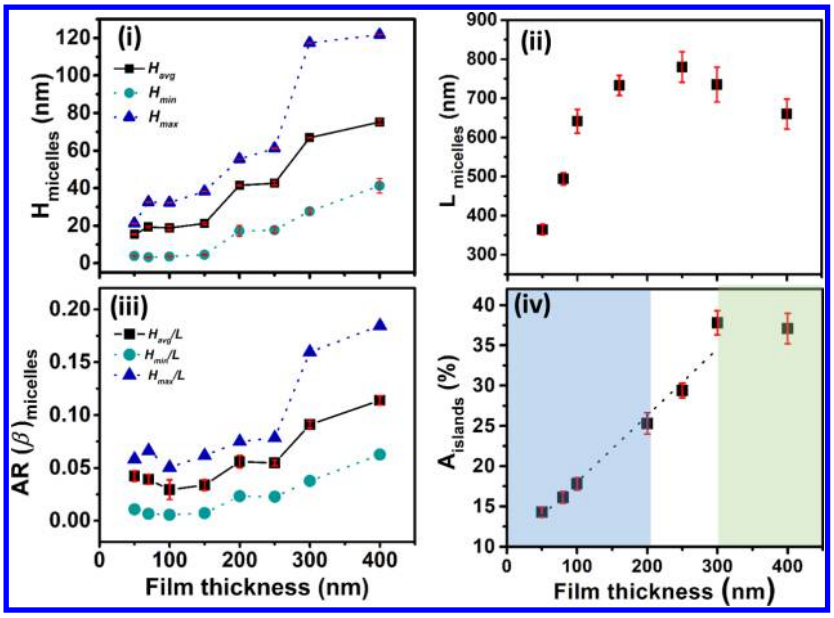


**Figure 6.** Effect of film thickness on (i) micelle height ($H$), (ii) lateral dimension of micelles ($L$), (iii) domain aspect ratio ($\beta$) with respect to $H$, and (iv) area fraction ($A$) of micelles. The blue-colored zone is the hydrophobic regime, and the green-colored zone is the hydrophilic regime. The transition regime is uncolored. Error bars represent standard error.

observed where the average size of the micelles (i.e., the hydrophilic domains) increased as the film thickness increased upto $h \approx 250$ nm and then went down , Figure 6(ii), discussed in detail later. The aspect ratio ($\beta$) of the domain was defined as the ratio of micelle height to the lateral dimension of the micelles. As the $\beta$ ($H_{micelles}/L_{micelles} < 1$), we conclude that these structures are 2D in nature. Additional information on film RMS roughness and micelle height relative to film thickness is available in SI Figure S2(i) & (ii).

Various studies have shown that the surface morphology influences the hydrophobicity of a surface.[51] The FDF films in the hydrophobic and hydrophilic regimes show high contact angle hysteresis and droplet pinning at 90° tilt, which is behavior characteristic of "sticky" surfaces (see SI Figure S3(i) for advancing and receding contact angles). Such surfaces tend to fall within the Wenzel regime wherein no air pockets are trapped between the surface topography feature and the liquid drop placed on it.[52] We note that Wenzel's[52] theory only applies to compositionally homogeneous surfaces, so it does not apply to our poly(DMA)/poly(FOSM) heterogeneous surface. Nevertheless, it provides a background for a starting interpretation of our results. According to Wenzel's[52] theory for hydrophobic surfaces, increasing roughness increases the hydrophobic nature of the surface. For the FDF films, however, the roughness is associated with hydrophilic poly(DMA) domains, and as the poly(DMA) domains became larger the roughness increased, as did the hydrophilic nature of the surface. We conclude the influence of roughness on the contact angle needs to be integrated with heterogeneity in surface chemistry, presently not accounted for in Wenzel's theory. It was observed that a hydrophobic solvent shows no contact angle variation on these heterogeneous surfaces, SI Figure S3(ii). Contact angle information for FDF films with different block lengths is also provided in SI Figure S3(iii), where films with a longer poly(DMA) block length show hydrophilic behavior irrespective of film thickness.

A poly(FOSM) homopolymer film exhibited a contact angle of 119.7°, which is not significantly different than that of the 40 nm BCP film, which indicates that for the film with the lowest size and surface density of poly(DMA) micellar domains, these distributed "wetting domains" were ignored from a macroscopic wetting perspective as reflected in contact angle, $\theta_c$. However, their importance grows as they become more dominant in thicker films. The lateral dimension of the hydrophilic poly(DMA) domains increased with increasing film thickness to a maximum value of $L \approx 740$ nm at $h = 250$ nm, and for even thicker films the average $L$ decreased, Figure 6(ii). We believe this is because once the poly(DMA) micellar domains reach a maximum size and density, any further increase can only occur by formation of smaller domains in addition to the larger ones (skewing the size distribution to reflect a decrease in average size), as seen in the AFM images and analysis in Figures 5 and 6, respectively. Expectedly, the area fraction of the hydrophilic domains increased with increasing film thickness, Figure 6(iv). While the domain size and surface area fraction of the poly(DMA) domains increased with increasing film thickness, the number density of domains decreased, a consequence of fixed available area, as shown in Figure 7. An important consequence of the overall surface morphology trend of micellar poly(DMA) domains is the observed abrupt transition in the surface wettability with varying film thickness. A decrease

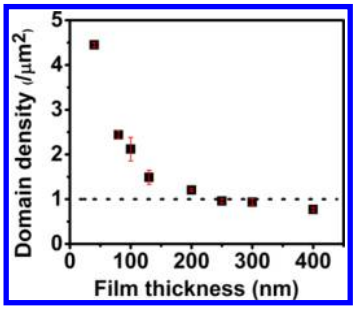


**Figure 7.** Domain density as a function of increasing film thickness. The dotted line represents a domain density of 1 domain/$\mu$m$^2$. Error bars represent standard error.


DOI: 10.1021/acsami.7b07245
ACS Appl. Mater. Interfaces 2017, 9, 35349−35359

in domain density while the coverage area of the micelles increased suggests that as the domains become more closely spaced, they may have contact and merge into fewer, but larger domains. That suggests a 2D percolation effect,[53] where a continuous network of poly(DMA) domains forms on the film surface.

As discussed earlier in the paper, the hydrophobic−hydrophilic transition was most easily observed for films between $h$ = 200 and 300 nm. The domain density of the poly(DMA) domains on the surface in 200 and 300 nm films was 1.24 and 0.93 domain/$\mu$m$^2$ respectively, with the crossover at 250 nm film with a domain density of 0.96 domain/$\mu$m$^2$ which suggests that the surface percolation of the hydrophilic poly(DMA) occurs for a domain density of ∼1 circular disc-like domain/$\mu$m$^2$. AFM results shown in Figure 5 however indicate that for all films, these wetting surface micellar domains were discrete and were not physically connected. This apparent discrepancy between surface percolation without direct connectivity may be reconciled if the mechanism for the hydrophobic to hydrophilic transition were a "jump-percolation", wherein the water droplets bridge the high density of the hydrophilic domains in close proximity to each other, overcoming the weakly interconnected hydrophobic poly(FOSM) background. The fact that the poly(DMA) domains have a vertical protrusion above the poly(FOSM) background is likely helpful to the jump-percolation process. This wetting is likely a dynamic process for the transition film thicknesses in the range of 200 to 300 nm, where the percolative poly(FOSM) competes with jump-percolation poly(DMA) micellar domains for determining overall film wettability.

Finally, as a demonstration of a possible multifunctional application, the diffuse scattering of light from these nanoroughened surfaces was evaluated. Since these films had surface domain sizes in the range of 350 to 750 nm and surface roughness in the range of 6 to 30 nm they can act as optical diffusers. Reflectance (or diffuse reflectance) of the FDF films increased linearly with increasing film thickness from 60 to 200 nm, Figure 8(i), which corresponded to surface domain sizes from 360 to 740 nm, Figure 6(ii). A preferable correlation was multiplying the domain size ($L_{micelles}$) by the RMS roughness,[54,55] Figure 8(ii), to obtain the nanoroughened area. In this case, the product of the domain size and the RMS roughness, provides an approximate measure of the scattering area.[56] That plot exhibits a linear relationship for all the film thicknesses considered in this research.

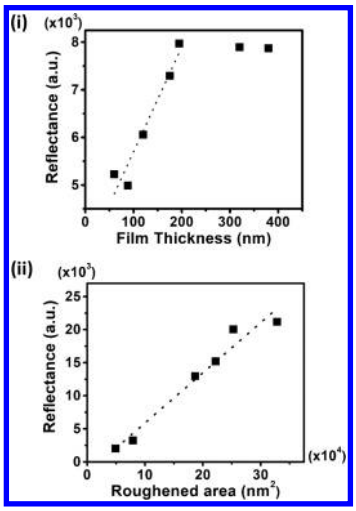


**Figure 8.** Diffuse reflectance as a function of (i) Film thickness and (ii) roughened area (RMS roughness × lateral dimension of micelles), indicate the optical properties of these nanoroughened surfaces.

Note that the 53% enhanced diffuse reflection (diffuse reflectance spectra and its wavelength dependence provided in SI Figure S5) from $h$ = 40 to $h$ = 200 nm in this system is mainly a consequence of the large refractive index (RI) difference between the poly(DMA) domains at the film surface and the surrounding air. The RIs of different components are $n_{poly(DMA)}$ = 1.64, $n_{poly(FOSM)}$ = 1.45, and $n_{FDF}$ (200 nm thick film) = 1.44, so the poly(DMA)/air interface has a high scattering contrast for light. Interestingly, it was observed that the diffuse reflectance values saturate at $h$ = 200 nm, which is also the onset of the transition zone. This interesting phenomenon merits future studies, that is however outside the scope of the current study.

## 3. CONCLUSIONS

Solvent cast thin film properties of an amphiphilic FDF triblock copolymer exhibit a natural confinement induced surface wettability transition that is correlated to a quasi 2D jump-percolation effect of critical wetting domain areal density in a monotonically decreasing nonwetting background. Molecularly, the wettability transition is ascribable to a threshold scale and chemical heterogeneity of phase separation of elevated hydrophilic poly(DMA) domains in a hydrophobic poly(FOSM) background matrix, whose size and density are determined by film thickness. We envision this interesting finite size effect induced transition can be tunable by the film's static and dynamic behavior via control of the surface wettability and phase behavior of its blend constituents and composition. Besides, interesting wetting properties, such films also have potentially useful film thickness dependent tunable light scattering properties for further application as multifunctional films.

## 4. METHODS

**4.1. Materials.** The synthesis of the FDF triblock copolymer, Figure 1, was previously described.[31] It involved a three-step sequential RAFT polymerization with a 2-cyano-2-propyl benzodithioate catalyst. The initial poly(FOSM) polymerization was carried out in $\alpha,\alpha,\alpha$-trifluorotoluene (TFT) solution and two subsequent polymerizations of poly(DMA) and poly(FOSM) were carried out in a solvent mixture of 3:1 (v/v) 1,4-dioxane and TFT. The specific FDF BCP used in this study was an asymmetric triblock copolymer with a volume fraction of FOSM of $\phi_{FOSM}$ = 0.579 and block molecular masses (kg/mol) of 16.0, 19.8, and 25.6, see Figure 1.

The dry BCP formed an alternating lamellae microstructure with a periodicity of 31 nm and the fluoroalkyl side chains formed a smectic bilayer with a spacing of 2.9 nm within the poly(FOSM) nanodomains.[31] When the BCP was swollen to equilibrium with water, the swelling ratio (mass gel/mass dry polymer) was 1.77 and the BCP microstructure changed to hexagonally packed cylindrical nanodomains with poly(FOSM) cylinders 7 nm in diameter and separated by 45 nm.

**4.2. Film Preparation and Characterization.** Thin polymer films were cast from hexafluoroisopropanol, HFIP, (boiling point at atmospheric pressure (∼101 kPa) is 58.2 °C) solutions onto silicon wafers that were treated immediately prior to use by ultraviolet ozone (UVO) for 1 h to attain a clean silica surface. The silicon wafers were obtained from University Wafers (Boston, MA), and the HFIP (≥99% purity) was obtained from Fischer Scientific and used as-received. The film casting was done by flow coating at room temperature (∼23 °C). Films with a gradient of thickness ($h$) were achieved by varying the


DOI: 10.1021/acsami.7b07245
ACS Appl. Mater. Interfaces 2017, 9, 35349−35359

flow coating velocity, where higher velocity produced thicker films. Postcasting, all films were dried in a vacuum oven at 40 °C for 4 h to eliminate any residual solvent. Film thickness was measured with a thin film interferometer (F-20 UV Thin Film Analyzer, Filmetrics, Inc.). Water contact angles on the films were measured with a ramé-hart 500-F1 contact angle goniometer (Succasunna, NJ).

The elemental composition of the film surface was determined by X-ray photoelectron spectroscopy (XPS) using a PHI 5000 VersaProbe II. Structural characterization of the film was achieved using X-ray reflectivity (XRR) at the National Institute of Standards and Technology (NIST), Gaithersburg, MD, and grazing incidence small-angle X-ray scattering (GISAXS) at Advanced Photon Source, Argonne National Laboratories, Lemont, IL. Corresponding data analysis was performed using Reflpak,[57] reflectometry software by NIST Center for Neutron Research and GIXSGUI[58] (grazing-incidence X-ray scattering data visualization, reduction and analysis), and a MATLAB toolbox. Full width at half-maximum (fwhm) for GISAXS was calculated by peak fitting using OriginPro 8.5. GISAXS measurements were made at various incident angles ranging from $\alpha$ = 0.1° to 0.3°. The critical angle $\alpha_c$ for FDF in air is 0.15°, so at lower $\alpha$, only the top few nm of the film were probed, and at $\alpha > \alpha_c$, the bulk of the film was being probed. The surface morphology of the samples was characterized using a Dimension Icon atomic force microscope, AFM (Bruker AXS) in tapping and contact modes. An unmodified cantilever (Silicon-tip on Nitride cantilever) with a nominal spring constant of 0.58 N/m was used for friction scans. Image analysis was performed using ImageJ open-source software from NIH. Statistical analysis of particles observed in the AFM micrographs was performed using the "graph" plugin for imageJ[59] and NanoScope Analysis v1.4. Diffuse reflectance measurements were performed using an integrating sphere (AvaSphere-50-REFL), consisting of a black glossy trap to exclude specular reflection. All reflectance measurements were performed relative to a diffuse WS-2 white standard tile from Avantes. For quantitative comparisons, the area under the reflectivity spectrum was calculated by integration over the range of visible light, i.e., 350 to 750 nm, for each sample. The refractive index ($n$) of the materials was measured using a variable angle spectroscopic ellipsometer (VASE, J.A. Woollam Co., M-200).

## ■ ASSOCIATED CONTENT

### Supporting Information

The Supporting Information is available free of charge on the ACS Publications website at DOI: 10.1021/acsami.7b07245.

GISAXS images for all film thickness, AFM friction measurements in varied RH environment, advancing and receding contact angle information, hydrophobic solvent contact angles, water contact angles on FDF BCP films of varying block length, surface modulus, and diffuse reflectance spectra provided (PDF)

## ■ AUTHOR INFORMATION


### Corresponding Authors

*E-mail: rweiss@uakron.edu (R.A.W.).
*E-mail: alamgir@uakron.edu (A.K.).

### ORCID

R. A. Weiss: 0000-0002-5700-6871
Alamgir Karim: 0000-0003-1302-9374

### Present Addresses

[§]State Key Laboratory of Fine Chemicals, Department of Polymer Science and Engineering, Dalian University of Technology, Dalian Liaoning 116024, China.
[‖]Biology Department, University of Ghent, Sint-Pietersnieuwstraat 25, Ghent, East Flanders 900, Belgium.
[⊥]Department of Chemical & Biomolecular Engineering, University of Houston, Houston, TX-77204−4004, USA.


### Notes

Certain commercial equipment, instruments, or materials (or suppliers, or software, etc.) are identified in this paper to foster understanding. Such identification does not imply recommendation or endorsement by the National Institute of Standards and Technology, nor does it imply that the materials or equipment identified are necessarily the best available for the purpose.
The authors declare no competing financial interest.

## ■ ACKNOWLEDGMENTS

R.A.W. acknowledges NSF-CMMI 1300212, while A.K. acknowledges NSF-DMR 1411046 for support of this work. The authors would like to thank R. Zhang and Z. Nikolov for select samples measured for XRR (NIST), and XPS (UAkron) respectively. The authors would like to thank Joseph Strzalka for help with GISAXS measurements at beamline 8-ID at Advanced Photon Source, Argonne National Laboratory, which was supported by the U.S. Department of Energy (DOE) Office of Science User, under contract no. DE-AC02-06CH11357.

## ■ REFERENCES


(1) Gao, L.; Mccarthy, T. J. A Perfectly Hydrophobic Surface ($\theta$ A/$\theta$ R) 180°/180°. *J. Am. Chem. Soc.* **2006**, *128*, 9052−9053.
(2) Kota, A. K.; Choi, W.; Tuteja, A. Superomniphobic Surfaces: Design and Durability. *MRS Bull.* **2013**, *38* (5), 383−390.
(3) Han, J. T.; Kim, S.; Karim, A. UVO-Tunable Superhydrophobic to Superhydrophilic Wetting Transition on Biomimetic Nanostructured Surfaces. *Langmuir* **2007**, *23*, 2608−2614.
(4) Chaudhury, M. K.; Whitesides, G. M. How to make water run uphill. *Science* **1992**, *256*, 1539−1541.
(5) Osicka, J.; Ilčiková, M.; Popelka, A.; Filip, J.; Bertok, T.; Tkac, J.; Kasak, P. Simple, Reversible, and Fast Modulation in Superwettability, Gradient, and Adsorption by Counterion Exchange on Self- Assembled Monolayer. *Langmuir* **2016**, *32*, 5491−5499.
(6) Pitt, G. W. Fabrication of a Continuous Wettability Gradient by Radio Frequency Plasma Discharge. *J. Colloid Interface Sci.* **1989**, *133* (1), 223−227.
(7) Wang, Y.; Wang, X.; Lai, C.; Hu, H.; Kong, Y.; Fei, B.; Xin, J. H. Biomimetic Water-Collecting Fabric with Light-Induced Superhydrophilic Bumps. *ACS Appl. Mater. Interfaces* **2016**, *8*, 2950−2960.
(8) Eifert, A.; Petit, J.; Baier, T.; Bonaccurso, E.; Hardt, S. Applied Surface Science Inscribing Wettability Gradients onto Polymer Substrates with Different Stiffness Using Corona Discharge in Point-to-Plane Geometry. *Appl. Surf. Sci.* **2015**, *330*, 104−110.
(9) Li, J. S.; Ueda, E.; Nallapaneni, A.; Li, L. X.; Levkin, P. A. Printable Superhydrophilic−Superhydrophobic Micropatterns Based on Supported Lipid Layers. *Langmuir* **2012**, *28*, 8286−8291.
(10) Wang, N.; Xiong, D.; Deng, Y.; Shi, Y.; Wang, K. Mechanically Robust Superhydrophobic Steel Surface with Anti- Icing, UV-Durability, and Corrosion Resistance Properties. *ACS Appl. Mater. Interfaces* **2015**, *7*, 6260−6272.
(11) Zhang, Y.; Cheng, J.; Yang, Z. Applied Surface Science Construction of Wettability Gradient Surface on Copper Substrate by Controlled Hydrolysis of Poly (Methyl Methacrylate − Butyl Acrylate) Films. *Appl. Surf. Sci.* **2014**, *315*, 163−168.
(12) Hanus, J.; Kylián, O.; Vaidulych, M.; Khalakhan, I.; Choukourov, A.; Biederman, H.; Hanuš, J.; Kuzminova, A.; Slavínská, D.; Petr, M. Surfaces With Roughness Gradient and Invariant Surface Chemistry Produced by Means of Gas Aggregation Source and Magnetron Sputtering. *Plasma Processes Polym.* **2016**, *13*, 663−671.
(13) Roy, S.; Bhandaru, N.; Das, R.; Harikrishnan, G.; Mukherjee, R. Thermally Tailored Gradient Topography Surface on Elastomeric Thin Films. *ACS Appl. Mater. Interfaces* **2014**, *6*, 6579−6588.

(14) Gao, L.; Mccarthy, T. J. The " Lotus Effect " Explained: Two Reasons Why Two Length Scales of Topography Are Important. *Langmuir* **2006**, *22*, 2966−2967.
(15) Bates, F. S.; Fredrickson, G. H. Block Copolymer Thermodynamics: Theory and Experiment. *Annu. Rev. Phys. Chem.* **1990**, *41* (1), 525−557.
(16) Segalman, R. A. Patterning with Block Copolymer Thin Films. *Mater. Sci. Eng., R* **2005**, *48*, 191−226.
(17) Berry, B. C.; Bosse, A. W.; Douglas, J. F.; Jones, R. L.; Karim, A. Orientational Order in Block Copolymer Films Zone Annealed below the Order-Disorder Transition Temperature. *Nano Lett.* **2007**, *7* (9), 2789−2794.
(18) Kataoka, K.; Yokoyama, M.; Yokoyama, M.; Sakurai, Y.; Kwon, G. S. Block Copolymer Micelles as Vehicles for Drug Delivery (L & J). *J. Controlled Release* **1993**, *24*, 119−132.
(19) Cho, J.; Hong, J.; Char, K.; Caruso, F. Nanoporous Block Copolymer Micelle/Micelle Multilayer Films with Dual Optical Properties. *J. Am. Chem. Soc.* **2006**, *128*, 9935−9942.
(20) Spatz, J. P.; Mössmer, S.; Hartmann, C.; Möller, M.; Ulm, D.; Herzog, T.; Krieger, M.; Boyen, H.; Ziemann, P.; Kabius, B. Ordered Deposition of Inorganic Clusters from Micellar Block Copolymer Films. *Langmuir* **2000**, *16*, 407−415.
(21) Ruardy, T. G.; Moorlag, H. E.; Schakenraad, J. M.; Van Der Mei, H. C.; Busscher, H. J. Growth of Fibroblasts and Endothelial Cells on Wettability Gradient Surfaces. *J. Colloid Interface Sci.* **1997**, *188* (188), 209−217.
(22) Lee, J. H.; Lee, H. B. Platelet Adhesion onto Wettability Gradient Surfaces in the Absence and Presence of Plasma Proteins. *J. Biomed. Mater. Res.* **1998**, *41* (2), 304−311.
(23) Liu, Q.; Xu, B. Actuating Water Droplets on Graphene *via* Surface Wettability Gradients. *Langmuir* **2015**, *31*, 9070−9075.
(24) Chakraborty, M.; Ghosh, U. U.; Chakraborty, S.; Dasgupta, S. *Thermally enhanced self-propelled droplet motion on gradient surfacesRSC Adv.* **2015**, *5*, 45266−45275.
(25) Farhat, N.; Alen, S. K.; Rahman, A. Numerical Study of the Wetting and Mobility of Liquid Droplets on Horizontal and Inclined Flat and Microgrooved Surfaces. *Procedia Eng.* **2015**, *105*, 576−585.
(26) Huang, J.; Huang, H.; Wang, X. Numerical Study of Drop Motion on a Surface with Stepwise Wettability Gradient and Contact Angle Hysteresis. *Phys. Fluids* **2014**, *26* (6), 1−45.
(27) Nakashima, Y.; Nakanishi, Y.; Yasuda, T. Automatic Droplet Transportation on a Plastic Microfluidic Device Having Wettability Gradient Surface. *Rev. Sci. Instrum.* **2015**, *86* (1), 015001.
(28) Gan, D.; Mueller, A.; Wooley, K. L. Amphiphilic and Hydrophobic Surface Patterns Generated from Hyperbranched Fluoropolymer/Linear Polymer Networks: Minimally Adhesive Coatings via the Crosslinking of Hyperbranched Fluoropolymers. *J. Polym. Sci., Part A: Polym. Chem.* **2003**, *41* (22), 3531−3540.
(29) Makal, U.; Wynne, K. J. Water Induced Hydrophobic Surface. *Langmuir* **2005**, *21* (9), 3742−3745.
(30) Imbesi, P. M.; Finlay, J. A.; Aldred, N.; Eller, M. J.; Felder, S. E.; Pollack, K. A.; Lonnecker, A. T.; Raymond, J. E.; Mackay, M. E.; Schweikert, E. A.; Clare, A. S.; Callow, J. A.; Callow, E.; Wooley, K. L. Polymer Chemistry Composition, Physical Properties and Anti-Biofouling Performance of Networks. *Polym. Chem.* **2012**, *3*, 3121−3131.
(31) Niu, H.; Wang, F.; Weiss, R. A. Hydrophobic/hydrophilic Triblock Copolymers: Synthesis and Properties of Physically Cross-Linked Hydrogels. *Macromolecules* **2015**, *48* (3), 645−654.
(32) Abdurrahmanoglu, S.; Can, V.; Okay, O. Design of High-Toughness Polyacrylamide Hydrogels by Hydrophobic Modification. *Polymer* **2009**, *50* (23), 5449−5455.
(33) Hao, J.; Weiss, R. A. Viscoelastic and Mechanical Behavior of Hydrophobically Modified Hydrogels. *Macromolecules* **2011**, *44*, 9390−9398.
(34) Picknett, R. G.; Bexon, R. The evaporation of sessile or pendant drops in still air. *J. Colloid Interface Sci.* **1977**, *61* (2), 336−350.
(35) Bourges-Monnier, C.; Shanahan, M. E. R. Influence of evaporation on contact angle. *Langmuir* **1995**, *11* (7), 2820−2829.
(36) Lee, H.; Alcaraz, M. L.; Rubner, M. F.; Cohen, R. E. Zwitter-Wettability and Antifogging Capabilities. *ACS Nano* **2013**, *7* (3), 2172−2185.
(37) Crowe-Willoughby, J. A.; Genzer, J. Formation and Properties of Responsive Siloxane-Based Polymeric Surfaces with Tunable Surface Reconstruction Kinetics. *Adv. Funct. Mater.* **2009**, *19* (3), 460−469.
(38) Vaidya, A.; Chaudhury, M. K. Synthesis and Surface Properties of Environmentally Responsive Segmented Polyurethanes. *J. Colloid Interface Sci.* **2002**, *249*, 235−245.
(39) Nurmi, L.; Holappa, S.; Nykänen, A.; Laine, J.; Ruokolainen, J.; Seppälä, J. Ultra-Thin Films of Cationic Amphiphilic poly(2-(Dimethylamino)ethyl Methacrylate) Based Block Copolymers as Surface Wettability Modifiers. *Polymer* **2009**, *50* (22), 5250−5261.
(40) Wang, Y.; Dong, Q.; Wang, Y.; Wang, H.; Li, G.; Bai, R. Investigation on RAFT Polymerization of a Y-Shaped Amphiphilic Fluorinated Monomer and Anti-Fog and Oil-Repellent Properties of the Polymers. *Macromol. Rapid Commun.* **2010**, *31* (20), 1816−1821.
(41) Theato, P.; Brehmer, M.; Conrad, L.; Frank, C. W.; Funk, L.; Yoon, D. Y.; Lüning, J. Surface Reorganization of an Amphiphilic Block Copolymer Film Studied by NEXAFS Spectroscopy. *Macromolecules* **2006**, *39* (7), 2592−2595.
(42) Haraguchi, K.; Li, H.; Okumura, N. Hydrogels with Hydrophobic Surfaces: Abnormally High Contact Angles for Water on PNIPA Nanocomposite Hydrogels. *Macromolecules* **2007**, *40*, 2299−2302.
(43) Haraguchi, K.; Li, H. Hydrophobic Surface Characteristics of Nanocomposite Hydrogels. *Macromol. Symp.* **2010**, *291−292*, 159−167.
(44) Haraguchi, K.; Li, H.; Song, L. Unusually High Hydrophobicity and Its Changes Observed on the Newly-Created Surfaces of PNIPA/Clay Nanocomposite Hydrogels. *J. Colloid Interface Sci.* **2008**, *326*, 41−50.
(45) Peters, R. D.; Yang, X. M.; Kim, T. K.; Sohn, B. H.; Nealey, P. F. Using Self-Assembled Monolayers Exposed to X-Rays To Control the Wetting Behavior of Thin Films of Diblock Copolymers. *Langmuir* **2000**, *16*, 4625−4631.
(46) Fowkes, F. M. Attractive Forces at Interfaces. *Ind. Eng. Chem.* **1964**, *56* (12), 40−52.
(47) Smilgies, D. M. Scherrer Grain-Size Analysis Adapted to Grazing-Incidence Scattering with Area Detectors. *J. Appl. Crystallogr.* **2009**, *42*, 1030−1034.
(48) Martinelli, E.; Agostini, S.; Galli, G.; Chiellini, E.; Glisenti, A.; Pettitt, M. E.; Callow, M. E.; Callow, J. A.; Graf, K.; Bartels, F. W. Nanostructured films of amphiphilic fluorinated block copolymers for fouling release application. *Langmuir* **2008**, *24*, 13138−13147.
(49) Sikka, M.; Singh, N.; Karim, A.; Bates, F. S.; Satija, S. K.; Majkrzak, C. F. Entropy-driven surface segregation in block copolymer melts. *Phys. Rev. Lett.* **1993**, *70* (3), 307.
(50) Walheim, S.; Böltau, M.; Mlynek, J.; Krausch, G.; Steiner, U. Structure Formation *via* Polymer Demixing in Spin-Cast Films. *Macromolecules* **1997**, *30* (17), 4995−5003.
(51) Quéré, D. Wetting and Roughness. *Annu. Rev. Mater. Res.* **2008**, *38*, 71−99.
(52) Wenzel, R. N. Resistance of Solid Surfaces to Wetting by Water. *Ind. Eng. Chem.* **1936**, *28*, 988−994.
(53) Fan, P.; Wang, L.; Yang, J. Threshold Carbon Materials with Quasi-Graphene Layers: The Dielectric, Percolation Properties and the Electronic Transport Mechanism. *Chin. Phys. B* **2013**, *22* (3), 037701.
(54) Poulin, P.; Fournier, A. A. Model for Anisotropic Reflection. *Comp. Graph.* **1990**, *24* (4), 273.
(55) Wang, N.; Chen, X.; Yang, Y.; Dong, J.; Wang, C.; Yang, G. Diffuse Reflection inside a Hexagonal Nanocavity. *Sci. Rep.* **2013**, *3*, 1298.
(56) Nallapaneni, A.; Shawkey, M. D.; Karim, A. Specular and Diffuse Reflectance of Phase- Separated Polymer Blend Films. *Macromol. Rapid Commun.* **2017**, *38*, 1−8.


DOI: 10.1021/acsami.7b07245
*ACS Appl. Mater. Interfaces* 2017, 9, 35349−35359

(57) Ankner, J. F.; Majkrzak, C. F. Subsurface profile refinement for neutron specular reflectivity. In *S.P.I.E. Conference Proceedings*; S.P.I.E.: Bellingham, WA, 1992; Vol. *1738*.
(58) Jiang, Z. *GIXSGUI*: a MATLAB toolbox for grazing-incidence X-ray scattering data visualization and reduction, and indexing of buried three-dimensional periodic nanostructured films. *J. Appl. Crystallogr.* **2015**, *48*, 917.
(59) https://imagej.net/plugins/graph/index.html.



DOI: 10.1021/acsami.7b07245
*ACS Appl. Mater. Interfaces* 2017, 9, 35349−35359